Available online at www.sciencedirect.com
SCIENCE DIRECT®
International Journal of Solids and Structures 43 (2006) 1669–1692
INTERNATIONAL JOURNAL OF SOLIDS and STRUCTURES
www.elsevier.com/locate/ijsolstr

On the uses of special crack tip elements in numerical rock fracture mechanics

Mohammad Fatehi Marji [a,*], Hasan Hosseini_Nasab [b,1], Amir Hossein Kohsary [c,1]

[a] *Faculty of Mining Engineering, Yazd University, Yazd, Iran*
[b] *Department of Industrial Engineering, Yazd University, Yazd, Iran*
[c] *Department Mining Engineering, Yazd University, Yazd, Iran*

Received 27 November 2004; received in revised form 22 April 2005
Available online 1 July 2005

Abstract

Numerical methods such as boundary element methods are widely used for the stress analysis in solid mechanics. These methods are also used for crack analysis in rock fracture mechanics. There are singularities for the stresses and displacements at the crack tips in fracture mechanics problem, which decrease the accuracy of the numerical results in areas very close to the crack ends. To overcome this, higher order elements and isoperimetric higher order elements have been used. Recently, special crack tip elements have been proposed and used in most of the numerical fracture mechanics models. These elements can drastically increase the accuracy of the results near the crack tips, but in most of the models only one special crack tip element has been used for each crack end. In this study the uses of higher order crack tip elements are discussed and a higher order displacement discontinuity method is used to investigate the effect of these elements on the accuracy of the results in some crack problems. The useful shape functions for two special crack tip elements, are derived and given in the text and appendix for both infinite and semi-infinite plane problems. In this analysis both Mode I and Mode II stress intensity factors are computed . Some example problems are solved and the computed results are compared with the results given in the literature. The numerical results obtained here are in good agreement with those cited in the literature. For the curved crack problem, the strain energy release rate, G can be calculated accurately in the vicinity of the crack tips by using the higher order displacement discontinuity method with a quadratic variation of displacement discontinuity elements and with two special crack tip elements at each crack end.

* Corresponding author. Tel.: +98 351 8225328; fax: +98 351 8216900/0098 351 8210699.
E-mail addresses: mfatehi@yazduni.ac.ir (M.F. Marji), hhn@yazduni.ac.ir (H. Hosseini_Nasab), kohsary@yahoo.com (A.H. Kohsary).
[1] Fax: +98 351 8210699.

0020-7683/$ - see front matter © 2005 Elsevier Ltd. All rights reserved.
doi:10.1016/j.ijsolstr.2005.04.042

Keywords: Rock fracture mechanics; Higher order elements; Special crack tip elements; Numerical methods

1. Introduction

In the fracture analysis of brittle substances (like most of the rocks), the Mode I and Mode II stress intensity factors can be calculated by numerical methods using ordinary element. The accuracy of the numerical results are increased by using isoparametric elements and crack tip elements (Ingraffea and Hueze, 1980; Ingraffea, 1983; Blandford et al., 1982; Ingraffea, 1987; Guo et al., 1990; Scavia, 1990; Hwang and Ingraffea, 2004). Boundary element method is one of the powerful numerical methods and has been extensively used in fracture mechanics (Aliabadi and Rooke, 1991; Aliabadi, 1998). Displacement discontinuity method is an indirect boundary element method which has been used for the analysis of crack problems related to rock fracture mechanics and in most cases the problem of crack tip singularities has been improved by the uses of one crack tip element for each crack tip (Guo et al., 1992; Scavia, 1992; Shen and Stephansson, 1994; Scavia, 1995; Tan et al., 1996; Carpinteri and Yang, 1997; Bobet, 2001; Stephansson, 2002). Recently higher order elements have been used to increase the accuracy of the numerical results (Crawford and Curran, 1982; Shou and Crouch, 1995).

In this paper the higher order displacement discontinuity method that was originally introduced for finite and infinite crack problems (Shou and Crouch, 1995) is extended to the half plane problems with traction free surfaces (Crouch and Starfield, 1983). The general series for the crack tip elements is discussed and the required modification for implementation of the higher order special crack tip elements are given in Appendix A. The mixed mode stress intensity factors (i.e. for Mode I and Mode II fractures, which are the most commonly fracture modes occur in rock fracture mechanics) are numerically computed. As most of rocks are brittle and weak under tension the Mode I fracture toughness K_{IC} (under plain strain condition) together with the maximum tangential stress fracture criterion (σ-criterion) introduced by Erdogan and Sih are used to predict the crack propagation direction (Erdogan and Sih, 1963). The three fundamental fracture criteria, the maximum tangential stress criterion (or σ-criterion), the maximum strain energy release rate criterion (or G-criterion) and the minimum strain energy density criterion (or S-criterion) or any modified form of these three criteria (e.g. F-criterion which is a modified form of G-criterion) have been mostly used to study the fracture behaviour of brittle materials (Ingraffea, 1983; Broek, 1989; Whittaker et al., 1992; Shen and Stephansson, 1994). All of these criteria have demonstrated that a crack in a plate under a general in-plane load does not initiate and propagate in its original plane, but rather crack initiation take place at an angle with respect to it. The Mode II fracture toughness, K_{IIC} predicted by σ-criterion and G-criterion are smaller than the Mode I fracture toughness, K_{IC}, but it is generally larger than the Mode I fracture toughness, K_{IC} predicted by S-criterion depending on the material parameter of the Poisson's ratio v (because S-criterion depends on v). The mixed modes I–II fracture problems in compression have been shown to be more complicated and also quite different from those under tension. Various existing fracture criteria have been applied to study the fracture problems in compression but the results are poorly correlated to the existing experimental data (Whittaker et al., 1992). Although in brittle substances like rocks Mode II fracture initiation and propagation plays an important role under certain loading conditions and Mode I fracture toughness K_{IC} is less than Mode II fracture toughness, K_{IIC}, but due to the weakness (low strength) of rock under tension, the rock breaks due to tensile and in most cases the condition of K_{IC} will prevail to that of K_{IIC} under pure tensile, pure shear, tension-shear and compression-shear loading conditions. Recently, a lot of work has been done on the application of Mode I, Mode II and mixed Mode fracture theories for rock type materials (Ingraffea, 1981; Atkinson et al., 1982; Huang and Wang, 1985; Zipf and Bieniawski, 1987; Ouchterlony, 1988; Swartz et al., 1988; Sun et al., 1990; Fowell, 1995; Pang,

Table 1
Mode I fracture toughness K_{IC} and Mode II fracture toughness K_{IIC} for some typical rocks (after Whittaker et al. (1992))

Rock type	K_{IC} (MPa $m^{1/2}$)	K_{IIC} (MPa $m^{1/2}$)
Basalt	2.27	1.878
Newhurst Granite	1.72	1.750
Welsh Limestone	0.85	0.960
Coarse-grained Sandstone	0.28	0.360
Fine-grained Sandstone	0.38	0.420
Dark gray Syenite	1.75	1.180
Grayish white Syenite	1.36	0.830

1995; Stephansson et al., 2001; Backers et al., 2002, 2003, 2004; Rao et al., 2003; Shen et al., 2004). The Mode I fracture toughness K_{IC} and Mode II fracture toughness K_{IIC} for some typical rocks are given in Table 1.

Most of the existing numerical tools are based on the continuum assumption and rock failure is predicted by means of plastic deformation. Some recent numerical codes simulate the effect of existing fractures explicitly, and some of them are designed to model the fracture initiation and propagation of individual cracks. The recent fracture codes like FRACOD have been used (based on some useful mixed fracture criteria like F-criterion) to model the fracture propagation mechanism in brittle materials like rock (Shen and Stephansson, 1994). In the present work a general higher order displacement discontinuity method implementing two crack tip elements for each crack end is used and based on the linear elastic fracture mechanics principles the mixed mode σ-criterion (Erdogan and Sih, 1963) is implemented in this numerical model to handle the fracture initiation and propagation mechanism in rock type material considering the finite, infinite, and semi-infinite bodies. The emphasises is made on the uses of two special crack tip elements which increase the accuracy of the computed Mode I and Mode II stress intensity factors near the crack ends. Two equal crack tip elements have been used for each crack tip and the results seem to be more accurate than using only one crack tip element (which has been used in most of the existing numerical codes). The formulation given in Appendix A are in a concised form for both infinite and semi-infinite plane problems.

The displacement discontinuity solution based on one and two special crack tip elements are thoroughly explained and the required formulations are derived and given in the text and the crack propagation analysis is accomplished by using the σ-criterion. This criterion compares the computed Mode I and Mode II stress intensity factors K_I and K_{II} with their corresponding material properties i.e. Mode I and Mode II fracture toughnesses K_{IC} and K_{IIC} (Guo et al., 1992; Scavia, 1992). It should be noted that any fracture criterion can be implemented in the proposed method to study the fracture behaviour of brittle materials. A 45° circular arc crack under biaxial tension has been solved to show the validity of the results obtained by using the higher order displacement discontinuity program TDQCR2 in which uses two special crack tip elements at each crack end. Comparing the numerical and analytical values (i.e. the values of strain energy release rate, G) calculated for this problem proves the validity and accuracy of the numerical results for curved crack problems too.

2. Higher order displacement discontinuity method

A displacement discontinuity element of length 2a along the x-axis is shown in Fig. 1(a), which is characterized by a general displacement discontinuity distribution $u(\varepsilon)$. By taking the u_x and u_y components of the general displacement discontinuity $u(\varepsilon)$ to be constant and equal to D_x and D_y respectively, in the

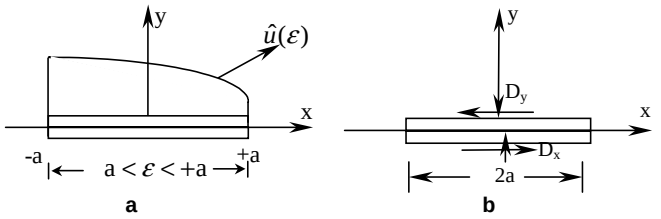

Fig. 1. (a) Displacement discontinuity element and the distribution of $u(\varepsilon)$; (b) constant element displacement discontinuity.

interval $(-a+a)$ as shown in Fig. 1(b), two displacement discontinuity element surfaces can be distinguished, one on the positive side of $y(y=0_+)$ and another one on the negative side $(y=0_-)$.

The displacement undergoes a constant change in value when passing from one side of the displacement discontinuity element to the other side. Therefore the constant element displacement discontinuities D_x and D_y can be written as

$$D_x = u_x(x,0_-) - u_x(x,0_+), \quad D_y = u_y(x,0_-) - u_y(x,0_+) \tag{1}$$

The positive sign convention of D_x and D_y is shown in Fig. 1(b) and demonstrates that when the two surfaces of the displacement discontinuity overlap D_y is positive, which leads to a physically impossible situation. This conceptual difficulty is overcome by considering that the element has a finite thickness, in its undeformed state which is small compared to its length, but bigger than D_y (Crouch, 1976; Crouch and Starfield, 1983).

2.1. Quadratic element formulation

The quadratic element displacement discontinuity is based on analytical integration of quadratic collocation shape functions over collinear, straight-line displacement discontinuity elements (Shou and Crouch, 1995). Fig. 2 shows the quadratic displacement discontinuity distribution, which can be written in a general form as

$$D_i(\varepsilon) = N_1(\varepsilon)D_i^1 + N_2(\varepsilon)D_i^2 + N_3(\varepsilon)D_i^3, \quad i = x,y \tag{2}$$

where, D_i^1, D_i^2, and D_i^3 are the quadratic nodal displacement discontinuities, and

$$N_1(\varepsilon) = \varepsilon(\varepsilon - 2a_1)/8a_1^2, \quad N_2(\varepsilon) = -(\varepsilon^2 - 4a_1^2)/4a_1^2, \quad N_3(\varepsilon) = \varepsilon(\varepsilon + 2a_1)/8a_1^2 \tag{3}$$

are the quadratic collocation shape functions using $a_1 = a_2 = a_3$. A quadratic element has three nodes, which are at the centers of its three sub-elements (see Fig. 2).

The displacements and stresses for a line crack in an infinite body along the x-axis, in terms of single harmonic functions $g(x,y)$ and $f(x,y)$, are given by Crouch and Starfield (1983) as

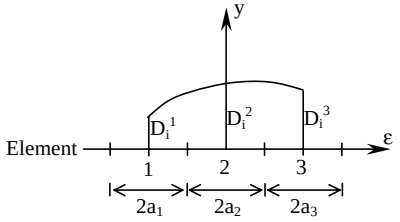

Fig. 2. Quadratic collocations for the higher order displacement discontinuity elements.

$$\begin{aligned} u_x &= [2(1-v)f_{,y} - yf_{,xx}] + [-(1-2v)g_{,x} - yg_{,xy}] \\ u_y &= [(1-2v)f_{,x} - yf_{,xy}] + [2(1-v)g_{,y} - yg_{,yy}] \end{aligned} \tag{4}$$

and the stresses are

$$\begin{aligned} \sigma_{xx} &= 2\mu[2f_{,xy} + yf_{,xyy}] + 2\mu[g_{,yy} + yg_{,yyy}] \\ \sigma_{yy} &= 2\mu[-yf_{,xyy}] + 2\mu[g_{,yy} - yg_{,yyy}] \\ \sigma_{xy} &= 2\mu[2f_{,yy} + yf_{,yyy}] + 2\mu[-yg_{,xyy}] \end{aligned} \tag{5}$$

μ is shear modulus and $f_{,x}$, $g_{,x}$, $f_{,y}$, $g_{,y}$, etc. are the partial derivatives of the single harmonic functions $f(x,y)$ and $g(x,y)$ with respect to x and y. These potential functions (for a quadratic variation of displacement discontinuity along the element) can be find from

$$f(x,y) = \frac{-1}{4\pi(1-v)} \sum_{j=1}^{3} D_x^j F_j(I_0, I_1, I_2), \quad g(x,y) = \frac{-1}{4\pi(1-v)} \sum_{j=1}^{3} D_y^j F_j(I_0, I_1, I_2) \tag{6}$$

the common function F_j, is defined as

$$F_j(I_0, I_1, I_2) = \int N_j(\varepsilon) \ln[(x-\varepsilon) + y^2]^{\frac{1}{2}} \mathrm{d}\varepsilon, \quad j = 1\text{–}3 \tag{7}$$

the integrals I_0, and I_1 and I_2 are expressed as

$$I_0(x,y) = \int_{-a}^{a} \ln[(x-\varepsilon)^2 + y^2]^{\frac{1}{2}} \mathrm{d}\varepsilon = y(\theta_1 - \theta_2) - (x-a)\ln(r_1) + (x+a)\ln(r_2) - 2a \tag{8.a}$$

$$I_1(x,y) = \int_{-a}^{a} \varepsilon \ln[(x-\varepsilon)^2 + y^2]^{\frac{1}{2}} \mathrm{d}\varepsilon = xy(\theta_1 - \theta_2) + 0.5(y^2 - x^2 + a^2)\ln\frac{r_1}{r_2} - ax \tag{8.b}$$

$$\begin{aligned} I_2(x,y) = \int_{-a}^{a} \varepsilon^2 \ln[(x-\varepsilon)^2 + y^2]^{\frac{1}{2}} \mathrm{d}\varepsilon &= \frac{y}{3}(3x^2 - y^2)(\theta_1 - \theta_2) + \frac{1}{3}(3xy^2 - x^3 + a^3)\ln(r_1) \\ &\quad - \frac{1}{3}(3xy^2 - x^3 - a^3)\ln(r_2) - \frac{2a}{3}\left(x^2 - y^2 + \frac{a^2}{3}\right) \end{aligned} \tag{8.c}$$

where, the terms θ_1, θ_2, r_1 and r_2 are defined as

$$\begin{aligned} &\theta_1 = \arctan\left(\frac{y}{x-a}\right), \quad \theta_2 = \arctan\left(\frac{y}{x+a}\right), \\ &r_1 = [(x-a)^2 + y^2]^{\frac{1}{2}} \quad \text{and} \quad r_2 = [(x+a)^2 + y^2]^{\frac{1}{2}} \end{aligned} \tag{9}$$

2.2. Higher order displacement discontinuity in a half-plane

Half-plane problems in solid mechanics can also be solved by infinite boundary element methods explained before, however, a more accurate and economic way for solving semi-infinite problems with a traction free surface, using the method of images, is originally introduced by Crouch and Starfield (1983) for the constant element displacement discontinuity method. They used the analytical solution to a constant element displacement discontinuity, over the line segment $|x| \leqslant a$, $y = 0$ in the semi-infinite region $y \leqslant 0$ as shown in Fig. 3. The displacements and stresses due to the actual displacement discontinuity are denoted

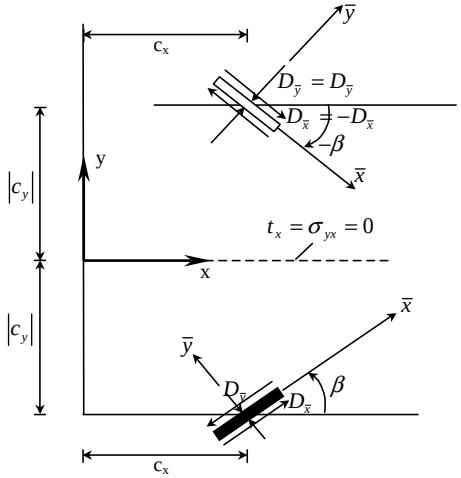

Fig. 3. Actual and image displacement discontinuities in half-plane $y \leqslant 0$, with a traction-free surface (Crouch and Starfield, 1983).

by u_i^{A} and σ_{ij}^{A}, those due to its image by u_i^{I} and σ_{ij}^{I}, and those resulting from the supplementary solution by u_i^{S} and σ_{ij}^{S}. The complete solution for the semi-infinite plane $y \leqslant 0$ can be written as

$$u_i = u_i^{\mathrm{A}} + u_i^{\mathrm{I}} + u_i^{\mathrm{S}} \quad \text{and} \quad \sigma_{ij} = \sigma_{ij}^{\mathrm{A}} + \sigma_{ij}^{\mathrm{I}} + \sigma_{ij}^{\mathrm{S}} \tag{10}$$

Based on these formulas and using quadratic element formulations explained in the previous section, a two dimensional semi-infinite displacement discontinuity computer program can be developed for the analysis of rock fracture mechanics problems, in which uses two special crack tip elements explained in the next section of this paper.

3. Higher order crack tip element formulation and stress intensity factor computation

The displacement discontinuity method permits the crack surfaces to be discretized and computes the crack opening displacement (normal displacement discontinuity), and crack sliding displacement (shear displacement discontinuity) directly as a part of the solution for each element. Due to the singularity variations $1/\sqrt{r}$, and $\sqrt{r}$ for the stresses and displacements near the crack ends, the accuracy of the displacement discontinuity method at the vicinity of the crack tip decreases, and usually a special treatment of the crack at the tip is necessary to increase the accuracy and make the method more efficient. In this study the hybrid elements are implemented in a general higher order displacement discontinuity method (i.e. the quadratic displacement discontinuity elements and two special crack tip elements for each crack end). Using a special crack tip element of length $2a$, as shown in Fig. 4, the displacement discontinuity variations along this element are given as

$$D_y(\varepsilon) = D_y(a)\left(\frac{\varepsilon}{a}\right)^{\frac{1}{2}} \quad \text{and} \quad D_x(\varepsilon) = D_x(a)\left(\frac{\varepsilon}{a}\right)^{\frac{1}{2}} \tag{11}$$

where ε is the distance from the crack tip and $D_y(a)$ and $D_x(a)$ are the opening and sliding displacement discontinuities at the center of the special crack tip element.

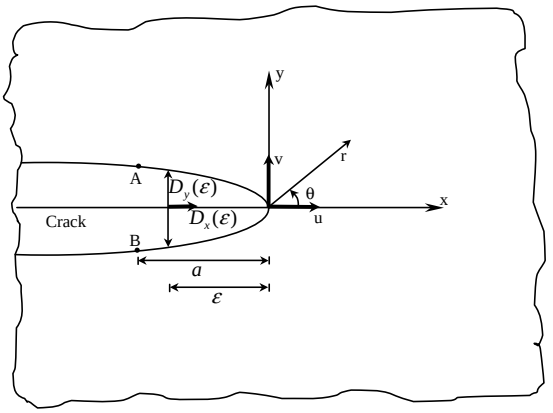

Fig. 4. Displacement correlation technique for the special crack tip element.

The potential functions $f_C(x,y)$ and $g_C(x,y)$ for the crack tip element can be expressed as

$$f_C(x,y) = \frac{-1}{4\pi(1-\nu)} \int_{=a}^{a} \frac{D_x(a)}{a^{\frac{1}{2}}} \varepsilon^{\frac{1}{2}} \ln[(x-\varepsilon)^2 + y^2]^{\frac{1}{2}} \mathrm{d}\varepsilon$$
$$g_C(x,y) = \frac{-1}{4\pi(1-\nu)} \int_{=a}^{a} \frac{D_y(a)}{a^{\frac{1}{2}}} \varepsilon^{\frac{1}{2}} \ln[(x-\varepsilon)^2 + y^2]^{\frac{1}{2}} \mathrm{d}\varepsilon \tag{12}$$

These equations have a common integral of the following form:

$$I_C = \int_{-a}^{a} \varepsilon^{\frac{1}{2}} \ln[(x-\varepsilon)^2 + y^2]^{\frac{1}{2}} \mathrm{d}\varepsilon \tag{13}$$

For the higher order crack tip elements the following series can be used (Crouch and Starfield, 1983):

$$D_i(\varepsilon) = C_1\varepsilon^{\frac{1}{2}} + C_2\varepsilon^{\frac{3}{2}} + C_3\varepsilon^{\frac{5}{2}} + \cdots \tag{14}$$

In order to use two crack tip elements the first two terms of Eq. (14) should be considered, which can be arranged in the following form:

$$D_i(\varepsilon) = [N_{C1}(\varepsilon)]D_i^1(a) + [N_{C2}(\varepsilon)]D_i^2(a) \tag{15}$$

The crack tip element has a length $a = a_2 + a_1$, and the shape functions $N_{C1}(\varepsilon)$ and $N_{C2}(\varepsilon)$ can be obtained as

$$N_{C1}(\varepsilon) = \frac{\left(a_2\varepsilon^{\frac{1}{2}} - \varepsilon^{\frac{3}{2}}\right)}{a_1^{\frac{1}{2}}(a_2 - a_1)} \quad \text{and} \quad N_{C2}(\varepsilon) = -\frac{\left(a_1\varepsilon^{\frac{1}{2}} - \varepsilon^{\frac{3}{2}}\right)}{a_2^{\frac{1}{2}}(a_2 - a_1)} \tag{16}$$

The potential functions $f_C(x,y)$ and $g_C(x,y)$ for the crack tip can be expressed as

$$f_C(x,y) = \frac{-1}{4\pi(1-\nu)} \int_{-a}^{a} D_x(\varepsilon) \ln[(x-\varepsilon)^2 + y^2]^{\frac{1}{2}} \mathrm{d}\varepsilon \tag{17.a}$$
$$g_C(x,y) = \frac{-1}{4\pi(1-\nu)} \int_{-a}^{a} D_y(\varepsilon)\varepsilon^{\frac{1}{2}} \ln[(x-\varepsilon)^2 + y^2]^{\frac{1}{2}} \mathrm{d}\varepsilon \tag{17.b}$$

inserting Eq. (16) in Eqs. (15) and (17), gives

$$f_C(x,y) = \frac{-1}{4\pi(1-v)}\left\{\left[\int_{-a}^{a} N_1(\varepsilon)\ln[(x-\varepsilon)^2+y^2]^{\frac{1}{2}}\,d\varepsilon\right]D_x^1 + \left[\int_{-a}^{a} N_2(\varepsilon)\ln[(x-\varepsilon)^2+y^2]^{\frac{1}{2}}\,d\varepsilon\right]D_x^2\right\} \quad (18.a)$$

$$f_C(x,y) = (I_{C1}(x,y)D_x^1 + I_{C2}(x,y)D_x^2)\left(-\frac{1}{4\pi(1-v)}\right) \quad (18.b)$$

$$f_C(x,y) = -\frac{1}{4\pi(1-v)}\sum_{j=1}^{2} D_x^j F_{Cj}(I_{C1},I_{C2}) \quad (18.c)$$

and similarly

$$g_C(x,y) = -\frac{1}{4\pi(1-v)}\sum_{j=1}^{2} D_y^j F_{Cj}(I_{C1},I_{C2}) \quad (19)$$

in which

$$F_{Cj}(I_{C1},I_{C2}) = \int_{-a}^{a} N_{Cj}(\varepsilon)\ln[(x-\varepsilon)^2+y^2]^{\frac{1}{2}}\,d\varepsilon, \quad j=1,2 \quad (20)$$

From Eq. (20) the following integrals are obtained:

$$\begin{aligned} I_{C1}(x,y) &= \int_{-a}^{a} \frac{a_2\varepsilon^{\frac{1}{2}} - \varepsilon^{\frac{3}{2}}}{a_1^{\frac{1}{2}}(a_2-a_1)}\ln[(x-\varepsilon)^2+y^2]^{\frac{1}{2}}\,d\varepsilon, \quad I_{C2}(x,y) \\ &= -\int_{-a}^{a} \frac{a_1\varepsilon^{\frac{1}{2}} - \varepsilon^{\frac{3}{2}}}{a_2^{\frac{1}{2}}(a_2-a_1)}\ln[(x-\varepsilon)^2+y^2]^{\frac{1}{2}}\,d\varepsilon \end{aligned} \quad (21)$$

These integrals can be arranged as

$$I_{C1}(x,y) = \frac{a_2}{d_{C1}}\overset{1}{I}_C - \frac{1}{d_{C1}}\overset{2}{I}_C \quad \text{and} \quad I_{C2}(x,y) = \frac{-a_1}{d_{C2}}\overset{1}{I}_C + \frac{1}{d_{C2}}\overset{2}{I}_C \quad (22)$$

where $d_{C1} = a_1^{\frac{1}{2}}(a_2-a_1)$, $d_{C2} = a_2^{\frac{1}{2}}(a_2-a_1)$, $\overset{1}{I}_C = \int_{-a}^{a}\varepsilon^{\frac{1}{2}}\ln[(x-\varepsilon)^2+y^2]^{\frac{1}{2}}\,d\varepsilon$, and

$$\overset{2}{I}_C = \int_{-a}^{a}\varepsilon^{\frac{3}{2}}\ln[(x-\varepsilon)^2+y^2]^{\frac{1}{2}}\,d\varepsilon \quad (23)$$

The derivations of integrals $\overset{1}{I}_C$ and $\overset{2}{I}_C$ which are used in the solution of the displacement discontinuities near the crack tip for both infinite and semi-infinite plane problems are given in Appendix A.

Several mixed mode fracture criteria has been used in literature to investigate the crack initiation direction and its path (Whittaker et al., 1992; Shen and Stephansson, 1994; Rao et al., 2003). The maximum tangential stress criterion (or σ-criterion), is the used here to investigate the crack initiation and propagation direction. This is a widely used mixed mode fracture criterion which is well fitted with the experimental results (Ingraffea, 1983; Guo et al., 1990; Scavia, 1992; Whittaker et al., 1992).

Based on LEFM theory, the Mode I and Mode II stress intensity factors K_I and K_{II} can be written in terms of the normal and shear displacement discontinuities as (Shou and Crouch, 1995):

$$K_I = \frac{\mu}{4(1-v)}\left(\frac{2\pi}{a}\right)^{\frac{1}{2}} D_y(a) \quad \text{and} \quad K_{II} = \frac{\mu}{4(1-v)}\left(\frac{2\pi}{a}\right)^{\frac{1}{2}} D_x(a) \quad (24)$$

4. Verification of higher order displacement discontinuity

Verification of this method is made through the solution of several example problems i.e. a pressurized crack in an infinite body, a circular arc crack under biaxial tension and circular holes with emanating cracks in infinite and semi-infinite bodies. These simple examples are used here because they have simple analytical solutions and have also been solved numerically by other researches, so that the computed numerical results in this paper can be compared and the validity of the proposed computer programs can be proved.

4.1. A pressurized crack in an infinite plane

Because of its simple solution, the problem of a pressurized crack have been used for the verification of the numerical methods developed here. The analytical solution of this problem has been derived and explained by Sneddon (1951). Based on Fig. 5, the analytical solution for the normal displacement discontinuity D_y along the crack boundary, and the normal stress σ_y near the crack tip ($|x| > b$), can be written as

$$D_y = -\frac{2(1-v)P}{\mu}(b^2 - x^2)^{\frac{1}{2}},\ |x| > b \quad \text{and} \quad \sigma_y = \frac{Px}{(x^2 - b^2)^{\frac{1}{2}}} - P,\ |x| < b \tag{25}$$

v is the Poisson's ratio of the body. Consider a pressurized crack of a half length $b = 1$ meter (m), under a normal pressure $P = -10$ MPa, with a modulus of elasticity $E = 2.2$ GPa, and a Poisson's ratio $v = 0.1$ (Fig. 5).

The normalized displacement discontinuity distribution $D_y/b \times 10^3$ along the surface of the pressurized crack are given in Table 2 using the constant (ordinary) displacement discontinuity program TWODD with different crack tip elements (Crouch and Starfield, 1983). As shown in this table by using only one special crack tip element, the percent error of displacement discontinuity D_y at a distance $x = 0.05b$ from the crack tip, reduces from 26.12 to 8.59, and by using two special crack tip elements it reduces to 5.07.

The same problem is solved by the higher order displacement discontinuity method (i.e. TWODQ program) using only 20 quadratic elements (60 nodes). The percentage error of displacement discontinuity D_y at a distance $x = 0.05b$ from the crack tip will be about 5.82% (with out using any special crack tip element) in which the results obtained by TWODD program with the same number of nodes (60 constant elements) gives an error of about 24.17%. Therefore using this higher order program for calculating the normalized

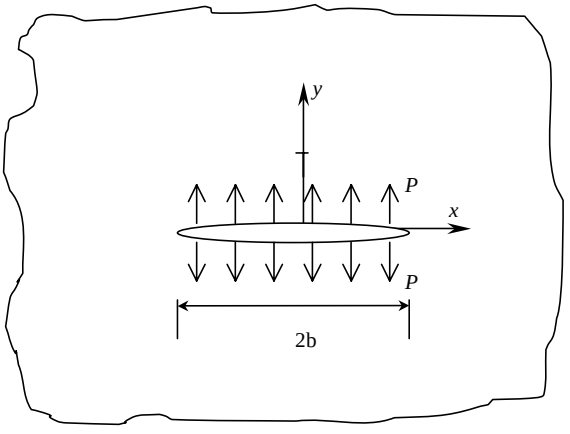

Fig. 5. A pressurized crack in an infinite body.

Table 2
Displacement discontinuity $D_y(a)$ at the center $x = a$ of an element at the crack tip using ordinary elements, one special crack tip element and two special crack tip elements

Number of elements	Distance from crack tip	$(D_y(a)/b) \times 10^3$			
		Analytical solution	Ordinary elements	One special crack tip element	Two special crack tip elements
4	0.25	−1.1906	−1.5463	−1.3275	−1.2150
10	0.1	−0.7846	−0.9964	−0.8569	−0.8202
20	0.05	−0.5621	−0.7089	−0.6104	−0.5906
40	0.025	−0.4000	−0.5029	−0.4332	−0.4212

displacement discontinuity distribution $D_y/b \times 10^3$ along the surface of the pressurized crack, gives more accurate results (see Table 3).

The normalized normal stress (σ_y/P) near the crack tip and along the x-axis of the pressurized crack is presented in Table 4. The over all results show that the program using quadratic elements (i.e. TWODQ) gives more accurate results compared to the program using constant elements (i.e. TWODD).

4.2. Curved cracks

Curved and kink cracks may occur in cracked bodies (Shou and Crouch, 1995). The proposed method is applied to the problem of a 45° circular arc crack under far field biaxial tension (Fig. 6). The program TDQCR2 (using quadratic displacement discontinuity elements with two special crack tip elements at each crack end) and the program TDQCR1 (using quadratic displacement discontinuity elements with only one special crack tip element at each crack end) have been developed for the analysis of the crack problems. Analytical values of the Mode I and Mode II stress intensity factors, K_I and K_{II}, and strain energy release rate, G for a general circular arc crack under biaxial tension given by Cotterell and Rice (1980) as

$$K_I = \sigma \cos\frac{\alpha}{4}\left[\frac{\pi r \sin\frac{\alpha}{2}}{1+\sin^2\frac{\alpha}{4}}\right]^{\frac{1}{2}}, \quad K_{II} = \sigma \sin\frac{\alpha}{4}\left[\frac{\pi r \sin\frac{\alpha}{2}}{1+\sin^2\frac{\alpha}{4}}\right]^{\frac{1}{2}} \quad \text{and} \quad G = \frac{1-\nu^2}{E}(K_I^2 + K_{II}^2) \tag{26}$$

Table 3
Comparison of variation of the displacement discontinuity $D_y/b \times 10^3$ along the surface of a pressurized crack using ordinary (constant) elements and higher order elements displacement discontinuity methods without using any special crack tip element

x/b	$D_y/b \times 1000$		
Distance from crack tip	Const. Elems. (TWODD)	Analytical results	Quad. Elems. (TWODQ)
0.0	4.046	3.980	3.980
0.086	4.032	3.946	3.966
0.171	3.989	3.901	3.922
0.257	3.916	3.827	3.848
0.343	3.812	3.720	3.741
0.429	3.673	3.578	3.599
0.514	3.497	3.396	3.419
0.600	3.276	3.168	3.193
0.686	3.000	2.882	2.909
0.771	2.654	2.520	2.556
0.857	2.203	2.040	2.094
0.950	1.536	1.237	1.309

Table 4
Variation of the normalized normal stress, σ_y/P near the crack tip and along the x-axis of the pressurized crack problem

$(x-b)/b$	σ_y/P		
	TWODD	ANALYTIC	Higher order elements
0.04	3.022	2.641	2.845
0.08	1.783	1.648	1.719
0.12	1.294	1.221	1.259
0.16	1.021	0.973	0.998
0.20	0.844	0.809	0.826
0.24	0.718	0.691	0.704
0.28	0.623	0.602	0.612
0.32	0.549	0.532	0.541
0.36	0.490	0.475	0.483
0.40	0.441	0.429	0.435

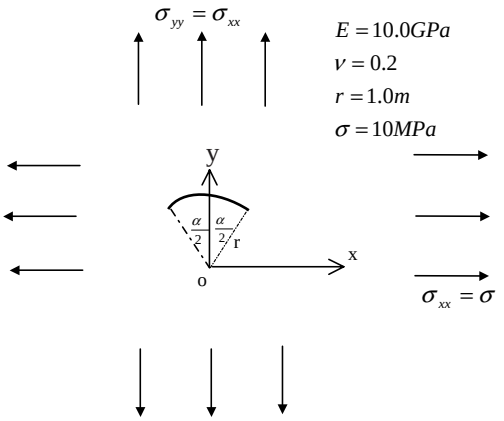

Fig. 6. Circular arc crack under uniform biaxial tension (Shou and Crouch, 1995).

Considering a circular arc crack ($\alpha = 45°$) under biaxial tension, $\sigma = 10$ MPa with a radius of $r = 1$ m. The modulus of elasticity and Poisson's ratio of the material are taken as $E = 10$ GPa and $v = 0.2$. The analytical values of the problem are obtained from Eq. (26) as $G = 11.47 \times 10^{-3}$ and based on the σ-criterion, the crack propagation angle, $\theta_0 = 20.90°$ (degrees) (Whittaker et al., 1992). The numerical solution of this problem have been obtained by using two higher order displacement discontinuity programs TDQCR1 (using one special crack tip element at each crack end), and TDQCR2 (using two special crack tip elements at each crack end). The numerical values for G and θ_0 are given in Tables 5 and 6; and Figs. 7 and 8, considering the two cases: (i) using a small crack tip element length L equal to 0.5° (i.e $L/b = 0.011$) and different number of nodes along the crack and (ii) using 60 nodes along the crack and different crack tip element length ratios (i.e. different L/b ratios). Comparing the numerical results of these two cases with the analytical results show that the results obtained by the program TDQCR2 are somewhat superior to those obtained by the program TDQCR1 specially when using relatively smaller number of nodes along the crack. The effect of L/b ratio on the results given by the program TDQCR2 is also negligible. Although the results obtained by both programs are in good agreement with the analytical results but in most cases the results obtained by the program TDQCR2 are preferred and can be used for the analysis of crack problems in rock fracture mechanics.

Table 5
The numerical values of the strain release rate, G for a circular arc crack ($\alpha = 45°$), using different number of nodes along the crack with a 0.5° crack tip

Number of nodes	The strain energy release rate $G \times 10^{-3}$		Crack initiation angle θ_0 (degrees)	
	TDQCR2	TDQCR1	TDQCR2	TDQCR1
6	18.92	23.82	23.13	22.58
12	13.99	16.44	21.57	21.57
18	12.55	14.25	21.17	21.26
24	11.94	13.24	21.01	21.12
30	11.61	12.68	20.93	21.05
36	11.43	12.34	20.90	20.99
42	11.32	12.11	20.88	20.96
48	11.27	11.94	20.86	20.93
54	11.21	11.82	20.85	20.92
60	11.20	11.73	20.85	20.91

Table 6
The numerical values of the strain release rate, G for a circular arc crack ($\alpha = 45°$), using different L/b ratios and 60 nodes along the crack

L/b ratio	The strain energy release rate $G \times 10^{-3}$	
	TDQCR2	TDQCR1
0.005	13.47	15.53
0.010	11.75	12.92
0.015	11.34	12.18
0.020	11.20	11.85
0.025	11.15	11.68
0.030	11.13	11.58
0.035	11.13	11.51
0.040	11.14	11.47

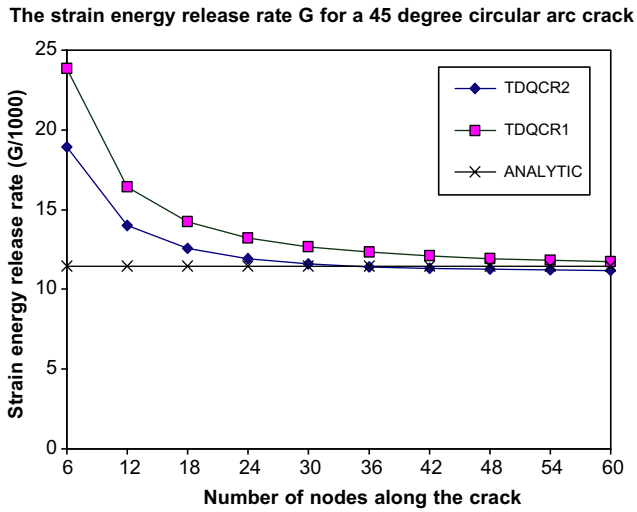

Fig. 7. The strain energy release rate, G for a circular arc crack ($\alpha = 45°$).

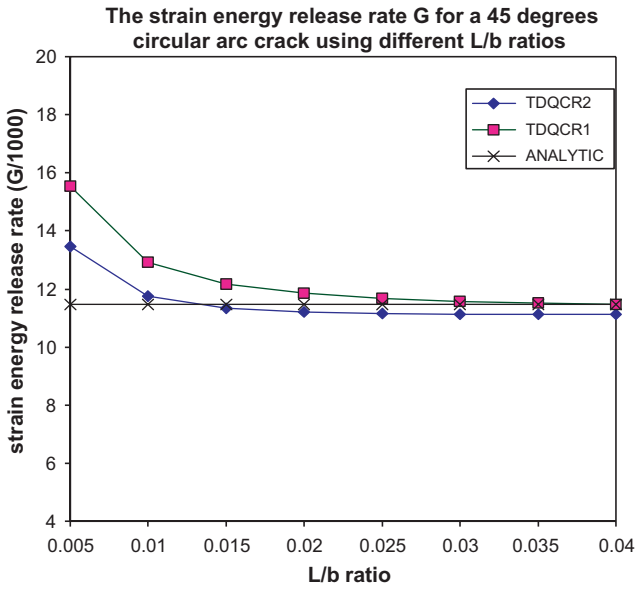

Fig. 8. The strain energy release rate, G for a circular arc crack ($\alpha = 45°$).

4.3. Circular holes with two emanating cracks

In order to show the benefit of both higher order elements and special crack tip elements explained above the example problem shown in Fig. 9 is solved numerically by the higher order displacement discontinuity method using quadratic displacement discontinuity elements for crack analysis (i.e. the programs TDQCR1 and TDQCR2). The following assumptions are made to solve this problem numerically: the far field stress $\sigma = 10$ MPa, the hole radius $R = 1$ m, modulus of elasticity $E = 10$ GPa, Poisson's ratio $\upsilon = 0.2$, and Mode I fracture toughness $K_{IC} = 2$ MPa $m^{1/2}$ (for a typical hard rock under plane strain condition).

The analytical value of the normalized stress intensity factor $K_I/(\sigma\sqrt{\pi b})$ obtained from the solutions given by Sih (1973) is about 1.96, for $b/R = 0.4$. The numerical result of the normalized stress intensity factor $K_I/(\sigma\sqrt{\pi b})$, for $b/R = 0.4$ using 90 nodes along the hole and 49 nodes along each crack, for different L/b ratios (i.e. the ratio of crack tip element length L to the crack length b) are shown graphically in Fig. 10.

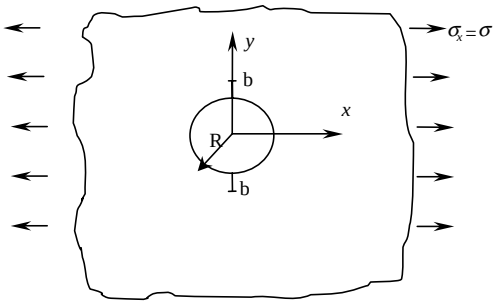

Fig. 9. A circular hole with two emanating cracks of length b under far field uniform tension.

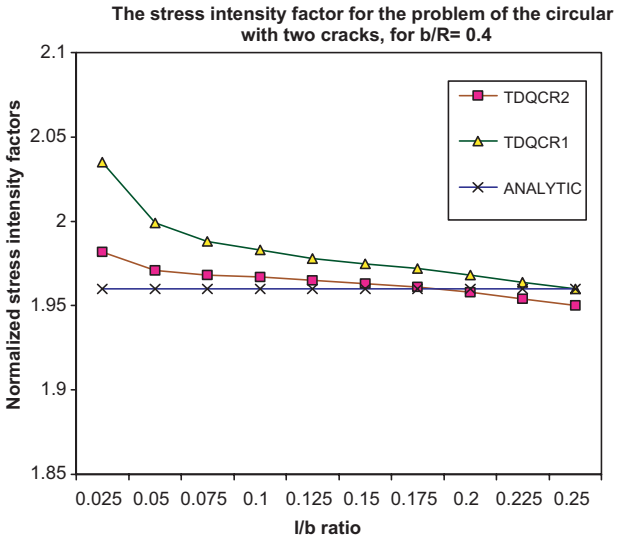

Fig. 10. The normalized stress intensity factor $K_1/(\sigma\sqrt{\pi b})$, for $b/R = 0.4$ and different l/b ratios.

The numerical results show that with L/b ratios between 0.1 and 0.2, the numerical results are accurate (in most cases the error is less than about 0.5%).

4.4. Crack problems in semi-infinite plane

The problem shown in Fig. 11 has been solved with the semi-infinite displacement discontinuity method using quadratic elements and special crack tip elements at each crack tip , considering the two limiting cases of pressurized circular holes having four cracks with (i) no pressure penetration (empty cracks), and (ii) full pressure penetration (fully pressurized cracks). The results of the normalized Mode I and Mode II stress

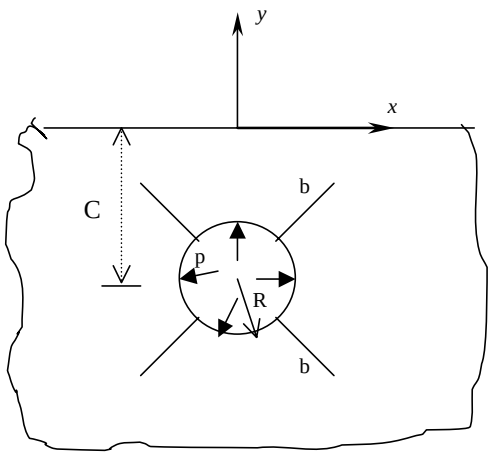

Fig. 11. A pressurized circular hole with four radial cracks at depth C in a semi-infinite body.

intensity factors $K_I/(p\sqrt{\pi\rho R})$, and $K_{II}/(p\sqrt{\pi\rho R})$, and the crack propagation angle θ_0, for these two extreme cases (i.e. empty cracks and fully pressurized cracks) against different normalized depths from the free surface of the half plane (C/R ratio), have been calculated numerically and given in Tables 7 and 8, respectively. All the results are numerically calculated by using 20 quadratic elements along the hole and 10 quadratic elements along each crack, with a constant value of $\rho = \frac{b+R}{R} = 2.5$, $R = 1$ m, and $p = \sigma = 10$ MPa. The analytical values of the normalized Mode I and Mode II stress intensity factors $K_I/(p\sqrt{\pi\rho R})$ and $K_{II}/(p\sqrt{\pi\rho R})$ and the crack initiation angle θ_0, for the problem of a pressurized circular hole with four symmetric radial cracks in a an infinite plane are given by Ouchterlony (1983) as: $K_I/(p\sqrt{\pi\rho R}) = 0.1966$, $K_{II}/(p\sqrt{\pi\rho R}) = 0.0$, and $\theta_0 = 0.0$ for the empty cracks; and $K_I/(p\sqrt{\pi\rho R}) = 0.9085$, $K_{II}/(p\sqrt{\pi\rho R}) = 0.0$, and $\theta_0 = 0.0$ for the fully pressurized cracks, respectively.

Table 7
The normalized stress intensity factors $K_I/(p\sqrt{\pi\rho R})$, and $K_{II}/(p\sqrt{\pi\rho R})$, and the crack propagation angle θ_0, for a pressurized hole with four empty radial cracks at different depths (C/R ratios)

C/R ratios	$K_I/(p\sqrt{\pi\rho R})$		$K_{II}/(p\sqrt{\pi\rho R})$		θ_0 (degrees)	
	Up. crack	Lo. crack	Up. crack	Lo. crack	Up. crack	Lo. crack
2.0	0.8473	0.4247	0.1056	0.0008	−13.8	−0.2
2.25	0.7068	0.3668	0.0644	−0.0196	−10.2	6.1
2.5	0.6053	0.3354	0.0633	−0.0250	−11.7	8.4
2.75	0.5196	0.3141	0.0593	−0.0270	−12.7	10.0
3.0	0.4527	0.2977	0.0533	−0.0290	−13.1	10.1
3.25	0.3959	0.2792	0.0462	−0.0256	−13.0	10.3
3.5	0.3592	0.2703	0.0418	−0.0254	−12.9	10.6
3.75	0.3245	0.2628	0.0326	−0.0250	−11.3	10.7
4.0	0.3086	0.2570	0.0267	−0.0240	−10.4	10.5
4.25	0.2808	0.2510	0.0227	−0.0230	−9.1	10.3
4.5	0.2686	0.2478	0.0176	−0.0208	−7.4	9.5
4.75	0.2565	0.2441	0.0128	−0.0199	−5.7	9.2
5.0	0.2477	0.2410	0.0106	−0.0187	−4.9	8.8

Table 8
The normalized stress intensity factors $K_I/(p\sqrt{\pi\rho R})$, and $K_{II}/(p\sqrt{\pi\rho R})$ and the crack propagation angle θ_0, for a pressurized hole under the uniform inside pressure p, with four fully pressurized radial cracks at different depths (C/R ratios)

C/R ratios	$K_I/(p\sqrt{\pi\rho R})$		$K_{II}/(p\sqrt{\pi\rho R})$		θ_0 (degrees)	
	Up. crack	Lo. crack	Up. crack	Lo. crack	Up. crack	Lo. crack
2.0	2.2036	1.3534	0.1954	0.0194	−10.0	−1.6
2.25	1.8940	1.2366	0.1230	−0.0307	−7.4	2.8
2.5	1.6993	1.1766	0.1285	−0.0465	−8.6	4.5
2.75	1.5298	1.1352	0.1229	−0.0565	−9.1	5.7
3.0	1.3937	1.1022	0.1109	−0.0626	−9.0	6.5
3.25	1.2690	1.0578	0.0949	−0.0552	−8.5	5.9
3.5	1.1927	1.0392	0.0862	−0.0573	−8.2	6.3
3.75	1.1116	1.0230	0.0609	−0.0587	−6.2	6.5
4.0	1.0344	1.0085	0.0470	−0.0580	−5.5	6.5
4.25	1.0114	0.9960	0.0362	−0.0573	−4.1	6.5
4.5	0.9863	0.9903	0.0223	−0.0523	−2.5	6.0
4.75	0.9582	0.9816	0.0091	−0.0510	−1.1	5.9
5.0	0.9390	0.9745	0.0044	−0.0487	−0.5	5.7

Figs. 12 and 13 are based on the normalized stress intensity factors given in the Tables 7 and 8, which compare the different results obtained for the upper cracks (the cracks near to the free surface of the half plane), and the lower cracks, with the available analytical results of the circular pressurized hole in an infinite plane (Ouchterlony, 1983). The numerical results show that as the depth of the circular pressurized hole (C/R ratio) increases the mixed mode stress intensity factors K_I and K_{II}, and the crack propagation angle θ_0 tend to their corresponding analytical values of the circular pressurized hole in an infinite plane.

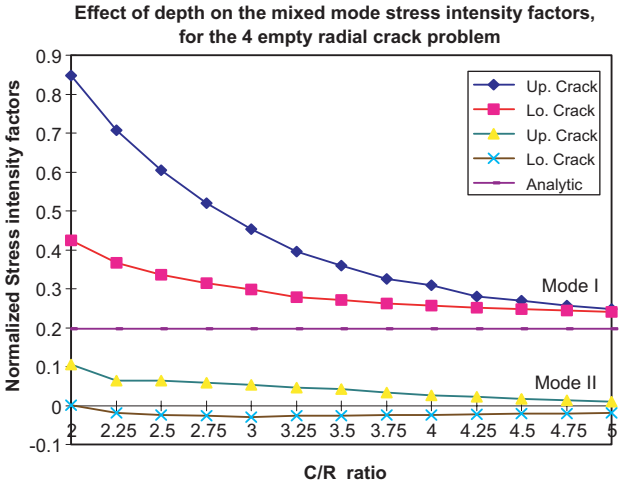

Fig. 12. The normalized stress intensity factors $K_I/(p\sqrt{\pi\rho R})$ and $K_{II}/(p\sqrt{\pi\rho R})$, for different C/R ratios, for a pressurized hole with four empty radial cracks in a semi-infinite rock mass.

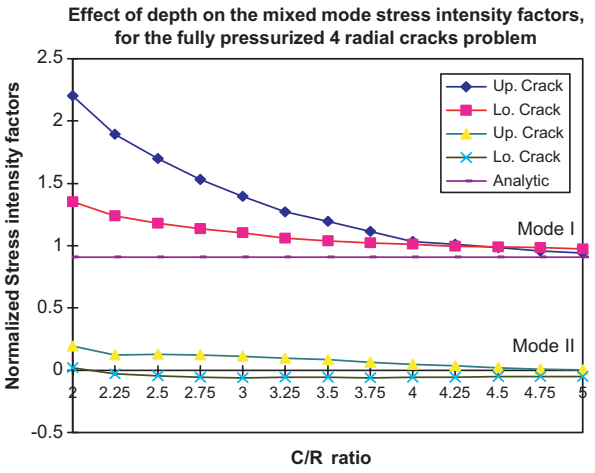

Fig. 13. The normalized stress intensity factors $K_I/(p\sqrt{\pi\rho R})$ and $K_{II}/(p\sqrt{\pi\rho R})$, for fully pressurized radial cracks emanating from a pressurized hole at different depths, in a semi-infinite rock mass.

5. Conclusion

The effect of using one and two special crack tip elements and also the effect of using higher order displacement discontinuity in two dimensional infinite and semi-infinite crack problems have been investigated. The complete and proper solutions and formulations are explained and given in the text and Appendix A. This method is modified to include, the finite, infinite, and semi-infinite problems using higher order (quadratic) displacement discontinuity elements. Several simple and mostly used example problems are selected and explained to verify the proposed modifications and improvements in the higher order displacement discontinuity method. At the end a somewhat more complicated and useful semi-infinite crack problem is solved and the numerical results are compared with the analytical values of the same problem in an infinite plane. It has been shown that as the depth of pressurized hole increases the problem changes to that of the infinite plane case. Therefore, it is concluded that the numerical results obtained by using the modified semi-infinite program gives very accurate results. This method is also modified for crack initiation and propagation analysis. Although any mixed mode fracture criterion can be implemented to this numerical code, but in this work, based on the linear elastic fracture mechanics (LEFM) principles, the maximum tangential stress criterion or σ-criterion is employed to investigate the crack initiation and propagation direction.

Appendix A. The integrals and their derivatives used for one and two special crack tip elements for both infinite and semi-infinite plane problems

A.1. The integral and its derivatives for one special crack tip element

$$I_c = \int_{-a}^{a} \varepsilon^{\frac{1}{2}} \ln[(x-\varepsilon)^2 + y^2]^{\frac{1}{2}} \, \mathrm{d}\varepsilon$$

$$I_{c,x} = \int_{-a}^{a} \frac{\varepsilon^{\frac{1}{2}}(x-\varepsilon)}{[(x-\varepsilon)^2 + y^2]} \, \mathrm{d}\varepsilon = xA_1 - A_2$$

$$I_{c,y} = \int_{-a}^{a} \frac{\varepsilon^{\frac{1}{2}} y}{[(x-\varepsilon)^2 + y^2]} \, \mathrm{d}\varepsilon = yA_1$$

$$I_{c,xy} = yA_{1,x}$$

$$I_{c,xx} = -A_1 - yA_{1,y} = -I_{c,yy}$$

$$I_{c,xyy} = A_{1,x} + yA_{1,xy}$$

$$I_{c,yyy} = 2A_{1,y} + yA_{1,yy}$$

The following formulae (derivatives) are also required for treatment of the traction free half-plane problems:

$$I_{c,xyyy} = 2A_{1,xy} + yA_{1,xyy}$$

$$I_{c,yyyy} = 3A_{1,yy} + yA_{1,yyy}$$

where, A_1, A_2, and the derivatives of A_1, are defined as

$$A_1 = \int_{-a}^{a} \frac{\varepsilon^{\frac{1}{2}}}{[(x-\varepsilon)^2 + y^2]} \mathrm{d}\varepsilon$$
$$= \rho^{-1} \left[0.5\left(\cos\varphi - \left(\frac{x}{y}\right)\sin\varphi\right) \ln\frac{2a - 2\sqrt{2a}\rho\cos\varphi + \rho^2}{2a + 2\sqrt{2a}\rho\cos\varphi + \rho^2} + \left(\sin\varphi + \left(\frac{x}{y}\right)\cos\varphi\right) \times \arctan\left(\frac{2\sqrt{2a}\rho\sin\varphi}{\rho^2 - 2a}\right) \right]$$

$$A_2 = \int_{-a}^{a} \frac{\varepsilon^{\frac{3}{2}}}{[(x-\varepsilon)^2 + y^2]} \mathrm{d}\varepsilon$$
$$= \rho \left[0.5\left(\cos\varphi + \left(\frac{x}{y}\right)\sin\varphi\right) \ln\frac{2a - 2\sqrt{2a}\rho\cos\varphi + \rho^2}{2a + 2\sqrt{2a}\rho\cos\varphi + \rho^2} + \left(\sin\varphi + \left(\frac{x}{y}\right)\cos\varphi\right) \times \arctan\left(\frac{2\sqrt{2a}\rho\sin\varphi}{\rho^2 - 2a}\right) \right]$$

where

$$\rho = (x^2 + y^2)^{\frac{1}{4}} \quad \text{and} \quad \varphi = 0.5\arctan\left(\frac{y}{x}\right)$$

and the derivatives of A_1 are

$$A_{1,x} = \rho^{-1} A1x1 - \frac{x}{2\rho^4} A_1$$
$$A_{1,y} = \rho^{-1} A1y1 - \frac{y}{2\rho^4} A_1$$
$$A_{1,xy} = \rho^{-1} A1x2 - \frac{y}{2\rho^5} A1x1 + \frac{xy}{\rho^8} A_1 - \frac{x}{2\rho^4} A_{1,y}$$
$$A_{1,yy} = \rho^{-1} A1y2 - \frac{y}{2\rho^5} A1y1 - \frac{x^2 - y^2}{2\rho^8} A_1 - \frac{y}{2\rho^4} A_{1,y}$$
$$A_{1,xyy} = \rho^{-1} A1x3 - \frac{y}{\rho^5} A1x2 - \frac{2x^2 - 3y^2}{2\rho^9} A1x1 + \frac{x^2 - 3y^2}{\rho^{12}} A_1 - \frac{2xy}{\rho^8} A_{1,y} - \frac{x}{2\rho^4} A_{1,yy}$$
$$A_{1,yyy} = \rho^{-1} A1y3 - \frac{y}{\rho^5} A1y2 - \frac{2x^2 - 3y^2}{2\rho^9} A1y1 + \frac{y(3x^2 - y^2)}{\rho^{12}} A_1 - \frac{x^2 - y^2}{\rho^8} A_{1,y} - \frac{y}{2\rho^4} A_{1,yy}$$

where

$$A1x1 = CN1 \times FLX + FL \times CN1X + CN2 \times TX + TC \times CN2X$$
$$A1y1 = CN1 \times FLY + FL \times CN1Y + CN2 \times TY + TC \times CN2Y$$
$$A1x2 = CN1 \times FLXY + FLX \times CN1Y + FL \times CN1XY + FLY \times CN1X + CN2 \times TXY + TX \times CN2Y + TY \times CN2X + TC \times CN2XY$$
$$A1y2 = CN1 \times FLYY + 2 \times FLY \times CN1Y + FL \times CN1YY + 2 \times TY \times CN2Y + CN2 \times TYY + TC \times CN2YY$$
$$A1x3 = CN1 \times FLXYY + 2 \times FLXY \times CN1Y + FLX \times CN1YY + 2 \times FLY \times CN1XY + FL \times CN1XYY + FLYY \times CN1X + 2 \times CN2Y \times TXY + CN2 \times TXYY + TX \times CN2YY + 2 \times CN2XY \times TY + TYY \times CN2X + TC \times CN2XYY$$
$$A1y3 = 3 \times CN1Y \times FLYY + CN1 \times FLYYY + 3 \times FLY \times CN1YY + FL \times CN1YYY + 3 \times CN2Y \times TYY + 3 \times TY \times CN2YY + CN2 \times TYYY + TC \times CN2YYY$$

The three form of terms *CN*s, *FL*'s, and *T*'s are necessary to be defined, for the above equations, and are given, respectively, in the following formulae.

(i) The terms *CN1*, *CN2*, *CN1X*, *CN2X*, etc. are defined as

$$CN1 = 0.5\left(\cos\varphi - \left(\frac{x}{y}\right)\sin\varphi\right)$$

$$CN2 = \sin\varphi + \left(\frac{x}{y}\right)\cos\varphi$$

$$CN1X = (CN1)_{,X} = 0.5(CP2 - (SNP + x \times SP2)/y)$$

$$CN1Y = (CN1)_{,y} = 0.5(CP3 - x \times SP3/y + x \times SNP/y^2)$$

$$CN1XY = (CN1)_{,xy} = 0.5(CP4 - (y \times SP3 - SNP - x \times SP2)/y^2 - x \times SP4/y), \text{ etc., and}$$

$$CN2X = (CN2)_{,X} = SP2 + (CSP + x \times CP2)/y$$

$$CN2Y = (CN1)_{,y} = SP3 - x \times (CSP - y \times CP3)/y^2$$

$$CN2XY = (CN2)_{,xy} = SP4 - (CSP + CP2)/y^2 + (CP3 + x \times CP4)/y, \text{ etc.},$$

where

$$SNP = \sin\varphi = \sin\left[0.5\arctan\left(\frac{y}{x}\right)\right]$$

$$CSP = \cos\varphi = \cos\left[0.5\arctan\left(\frac{y}{x}\right)\right]$$

$$CP2 = (\cos\varphi)_{,x} = y \times SNP/(2\rho^4)$$

$$CP3 = (\cos\varphi)_{,y} = -x \times SNP/(2\rho^4)$$

$$CP4 = (\cos\varphi)_{,xy} = (2(x^2 - y^2) \times SNP + xy \times CSP)/(4\rho^8), \text{ etc.},$$

and

$$SP2 = (\sin\varphi)_{,x} = -y \times CSP/(2\rho^4)$$

$$SP3 = (\sin\varphi)_{,y} = x \times CSP/(2\rho^4)$$

$$SP4 = (\sin\varphi)_{,xy} = (2(y^2 - x^2) \times CSP + xy \times SNP)/(4\rho^8), \text{ etc.}$$

(ii) The terms *FL*, *FLX*, *FLY*, etc. are defined as

$$FL = \ln(DL1/DL2)$$

$$FLX = FL1X - FL2X$$

$$FLY = FL1Y - FL2Y$$

$$FLXY = FL1XY - FL2XY, \text{etc.},$$

where

$$FL1X = DL1X/DL1$$

$$FL2X = DL2X/DL2$$

$$FL1XY = (FL1X)_{,y} = -DL1Y \times DL1X/(DL1)^2 + DL1XY/DL1$$

$$FL2XY = (FL2X)_{,y} = -DL2Y \times DL2X/(DL2)^2 + DL2XY/DL2, \text{ etc.},$$

with

$$DL1 = 2a - 2\sqrt{2a}\rho\cos\varphi + \rho^2$$
$$DL1X = (DL1)_{,x} = -\sqrt{2a}[x \times CSP/\rho^3 + y \times SNP/\rho^3] + x/\rho^2$$
$$DL1Y = (DL1)_{,y} = -\sqrt{2a}[y \times CSP/\rho^3 - x \times SNP/\rho^3] + y/\rho^2$$
$$DL1XY = (DL1)_{,xy} = -\sqrt{2a}[-2xy \times CSP + (x^2 - y^2) \times SNP]/(2\rho^7) - xy/\rho^6, \text{etc., and}$$
$$DL2 = 2a + 2\sqrt{2a}\rho\cos\varphi + \rho^2$$
$$DL2X = (DL2)_{,x} = \sqrt{2a}[x \times CSP/\rho^3 + y \times SNP/\rho^3] + x/\rho^2$$
$$DL2Y = (DL2)_{,y} = \sqrt{2a}[y \times CSP/\rho^3 - x \times SNP/\rho^3] + y/\rho^2$$
$$DL2XY = (DL2)_{,xy} = \sqrt{2a}[-2xy \times CSP + (x^2 - y^2) \times SNP]/(2\rho^7) - xy/\rho^6, \text{etc.}$$

(iii) The terms TC, TX, TY, TXY, TYY, etc. are defined as

$$TC = \arctan\frac{2\sqrt{2a}\rho\sin\varphi}{\rho^2 - 2a}, \quad \text{and}$$
$$TX = DT1/DT$$
$$TY = DT2/DT$$
$$TXY = (TX)_{,y} = -DTY \times DT1/(DT)^2 + DT1Y/DT$$
$$TYY = (TY)_{,y} = -DTY \times DT2/(DT)^2 + DT2Y/DT, \text{ etc.,}$$

where

$$DT = \rho^4 - 4a\rho^2\cos 2\varphi + 4a^2$$
$$DTY = 2y - 4a(y\cos 2\varphi - x\sin 2\varphi)/\rho^2$$
$$DTYY = 2,$$

$$DT1 = 2\sqrt{2a}[RY1 \times PY1 + RY2 \times PY2]$$
$$DT1Y = (DT1)_{,y} = 2\sqrt{2a}[-RY11 \times PY1 - RY1 \times PY11 + RY21 \times PY2 + RY2 \times PY21] \text{ and}$$
$$DT1YY = (DT1)_{,yy}$$
$$= 2\sqrt{2a}[-RY12 \times PY1 - 2RY11 \times PY11 - RY1 \times PY12 + RY22 \times PY2 + 2RY21 \times PY21 + RY2 \times PY22]$$
$$DT2 = 2\sqrt{2a}[RY1 \times PY4 - RY2 \times PY3]$$
$$DT2Y = (DT2)_{,y} = 2\sqrt{2a}[RY11 \times PY4 + RY1 \times PY41 - RY21 \times PY3 - RY2 \times PY31] \text{ with}$$
$$DT2YY = (DT2)_{,yy}$$
$$= 2\sqrt{2a}[RY12 \times PY4 + 2RY11 \times PY41 + RY1 \times PY42 - RY22 \times PY3 - 2RY21 \times PY31 - RY2 \times PY32]$$

$$PY1 = y \times CSP + x \times SNP$$
$$PY2 = y \times CSP - x \times SNP$$
$$PY3 = x \times CSP + y \times SNP$$
$$PY4 = x \times CSP - y \times SNP$$

$$PY12 = CSP + x \times PY4/(2\rho^4)$$

$$PY12 = -x \times SNP/\rho^4 - \frac{4xy \times PY4 + x^2 \times PY1}{4\rho^8}$$

$$PY21 = CSP - x \times PY3/(2\rho^4)$$

$$PY22 = -x \times SNP/\rho^4 + \frac{4xy \times PY3 - x^2 \times PY2}{4\rho^8}$$

$$PY31 = SNP + x \times PY2/(2\rho^4)$$

$$PY32 = x \times CSP/(2\rho^4) - \frac{xy \times PY2}{\rho^8} + \frac{x \times PY21}{2\rho^4}$$

$$PY41 = -SNP - x \times PY1/(2\rho^4)$$

$$PY42 = -x \times (CSP + PY11)/(2\rho^4) + \frac{xy \times PY1}{\rho^8} \quad \text{and}$$

$$RY1 = \frac{1}{2\rho}, \quad RY11 = \frac{-y}{4\rho^5}, \quad RY12 = \frac{-2\rho^4 + 5y^2}{8\rho^9}$$

$$RY2 = \frac{a}{\rho^3}, \quad RY21 = \frac{-3ay}{2\rho^7}, \quad RY22 = \frac{-3a(2\rho^4 - 7y^2)}{4\rho^{11}}$$

A.2. The integrals and their derivatives for two special crack tip elements

Starting with the integrals $\overset{1}{I}_C$ and $\overset{2}{I}_C$ given in Section 3, the first integral $\overset{1}{I}_C = I_c$ and its derivatives are the same as those given in A.1 of this appendix. The integral $\overset{2}{I}_C$ and its derivatives are as follows:

$$\overset{2}{I}_C = \int_{-a}^{a} \varepsilon^{\frac{3}{2}} \ln[(x-\varepsilon)^2 + y^2]^{\frac{1}{2}} d\varepsilon$$

$$\overset{2}{I}_{C,x} = \int_{-a}^{a} \frac{\varepsilon^{\frac{3}{2}}(x-\varepsilon)}{[(x-\varepsilon)^2 + y^2]} d\varepsilon = x \int_{-a}^{a} \frac{\varepsilon^{\frac{3}{2}}}{[(x-\varepsilon)^2 + y^2]} d\varepsilon - \int_{-a}^{a} \frac{\varepsilon^{\frac{5}{2}}}{[(x-\varepsilon)^2 + y^2]} d\varepsilon = xA_2 - A_3$$

$$\overset{2}{I}_{C,y} = \int_{-a}^{a} \frac{\varepsilon^{\frac{3}{2}} y}{[(x-\varepsilon)^2 + y^2]} d\varepsilon = y \int_{-a}^{a} \frac{\varepsilon^{\frac{3}{2}}}{[(x-\varepsilon)^2 + y^2]} d\varepsilon = yA_2$$

$$\overset{2}{I}_{C,xy} = yA_{2,x}$$

$$\overset{2}{I}_{C,yy} = yA_{2,y} + A_2$$

$$\overset{2}{I}_{C,xyy} = yA_{2,xy} + A_{2,x}$$

$$\overset{2}{I}_{C,yyy} = yA_{2,yy} + 2A_{2,y}$$

and for the semi-infinite case the following derivatives are also needed:

$$\overset{2}{I}_{C,xyyy} = yA_{2,xyy} + 2A_{2,xy}$$

$$\overset{2}{I}_{C,yyyy} = yA_{2,yyy} + 3A_{2,yy}$$

where, A_1 and its derivatives are given in section A of this appendix, A_3 and, A_2 and its derivatives which needed for infinite and semi-infinite plane problems, are given as

$$A_3 = \int_{-a}^{a} \frac{\varepsilon^{\frac{5}{2}}}{[(x-\varepsilon)^2 + y^2]} \mathrm{d}\varepsilon = -\frac{2}{3}(2a)^{\frac{3}{2}} + 2xA_2 - (x^2+y^2)A_1$$

and A_2 and its derivatives can be written as

$$A_2 = \int_{-a}^{a} \frac{\varepsilon^{\frac{3}{2}}}{[(x-\varepsilon)^2 + y^2]} \mathrm{d}\varepsilon = 2(2a)^{\frac{1}{2}} + \frac{x^2+y^2}{2y}(\theta_1 - \theta_2) + 2xA_1 = 2(2a)^{\frac{1}{2}} + \frac{x^2+y^2}{2y} I_{0,y} + 2xA_1$$

$$A_{2,x} = \frac{x^2+y^2}{2y} I_{0,xy} + \frac{x}{y} I_{0,y} + 2xA_{1,x} + 2A_1$$

$$A_{2,y} = \frac{x^2+y^2}{2y} I_{0,yy} + \frac{y^2-x^2}{2y^2} I_{0,y} + 2xA_{1,y}$$

$$A_{2,xy} = \frac{x^2+y^2}{2y} I_{0,xyy} + \frac{y^2-x^2}{2y^2} I_{0,xy} + \frac{x}{y} I_{0,yy} - \frac{x}{y^2} I_{0,y} + 2xA_{1,xy} + 2A_{1,y}$$

$$A_{2,yy} = \frac{x^2+y^2}{2y} I_{0,yyy} + 2\frac{y^2-x^2}{2y^2} I_{0,yy} + \frac{x^2}{y^3} I_{0,y} + 2xA_{1,yy}$$

$$A_{2,xyy} = \frac{x^2+y^2}{2y} I_{0,xyyy} + 2\frac{y^2-x^2}{2y^2} I_{0,xyy} + \frac{x^2}{y^3} I_{0,xy} + \frac{x}{y} I_{0,yyy} - 2\frac{x}{y^2} I_{0,yy} + 2xA_{1,xyy} + 2A_{1,yy}$$

$$A_{2,yyy} = \frac{x^2+y^2}{2y} I_{0,yyyy} + 3\frac{y^2-x^2}{2y^2} I_{0,yyy} + 3\frac{x^2}{y^3} I_{0,yy} - \frac{3x^2}{y^4} I_{0,y} + 2xA_{1,yyy}$$

and for the semi-infinite case the following derivatives are also needed:

$$A_{2,xyyy} = \frac{x^2+y^2}{2y} I_{0,xyyyy} + 3\frac{y^2-x^2}{2y^2} I_{0,xyyy} + \frac{3x^2}{y^3} I_{0,xyy} - \frac{3x^2}{y^4} I_{0,xy} + \frac{x}{y} I_{0,yyyy} - \frac{3x}{y^2} I_{0,yyy} + \frac{6x}{y^3} I_{0,yy} - \frac{6x}{y^4} I_{0,y} + 2xA_{1,xyyy} + 2A_{1,yyy}$$

$$A_{2,yyyy} = \frac{x^2+y^2}{2y} I_{0,yyyyy} + 4\frac{y^2-x^2}{2y^2} I_{0,yyyy} + \frac{6x^2}{y^3} I_{0,yyy} - \frac{12x^2}{y^4} I_{0,yy} + \frac{12x^2}{y^5} I_{0,y} + 2xA_{1,yyyy}$$

where

$$I_0 = \int_{-a}^{a} \ln[(x-\varepsilon)^2 + y^2]^{\frac{1}{2}} \mathrm{d}\varepsilon = y(\theta_1 - \theta_2) - (x-a)\ln(r_1) + (x+a)\ln(r_2) - 2a$$

$$I_{0,x} = \frac{\partial I_0}{\partial x} = \ln r_1 - \ln r_2$$

$$I_{0,y} = \theta_1 - \theta_2$$

$$I_{0,xy} = -\left(\frac{y}{r_1^2} - \frac{y}{r_2^2}\right)$$

$$I_{0,xx} = -\left(\frac{(x-a)}{r_1^2} - \frac{(x+a)}{r_2^2}\right) = -I_{0,yy}$$

$$I_{0,xyy} = -\left(\frac{(x-a)^2 - y^2}{r_1^4} - \frac{(x+a)^2 - y^2}{r_2^4}\right) = -I_{0,xxx}$$

$$I_{0,yyy} = -2y\left(\frac{(x-a)}{r_1^4} - \frac{(x+a)}{r_2^4}\right) = -I_{0,xxy}$$

$$I_{0,xyyy} = -2\left(\frac{(x-a)(r_1^2 - 4y^2)}{r_1^6} - \frac{(x+a)(r_1^2 - 4y^2)}{r_2^6}\right)$$

$$I_{0,yyyy} = 2y\left(\frac{3(x-a)^2 - y^2}{r_1^6} - \frac{3(x+a)^2 - y^2}{r_2^6}\right)$$

and for the semi-infinite case the following derivatives are also needed:

$$I_{0,xyyyy} = 24y\left(\frac{(x-a)((x-a)^2-y^2)}{r_1^8} - \frac{(x+a)((x+a)^2-y^2)}{r_2^8}\right)$$

$$I_{0,yyyyy} = \frac{I_{0,yyyy}}{y} - 8y^2\left(\frac{5(x-a)^2-y^2}{r_1^8} - \frac{5(x+a)^2-y^2}{r_2^8}\right)$$

The terms θ_1, θ_2, r_1 and r_2 are defined in Eq. (9) in Section 2.1.

References

Aliabadi, M.H., 1998. Fracture of Rocks. Computational Mechanics Publications, Southampton, UK.

Aliabadi, M.H., Rooke, D.P., 1991. Numerical Fracture Mechanics. Computational Mechanics Publications, Southampton, UK.

Atkinson, C., Smelser, R.E., Sanchez, J., 1982. Combined mode fracture via the cracked Brazilian disc test. Int. J. Fract. 18, 279–291.

Backers, T., Stephansson, O., Rybacki, E., 2002. Rock fracture toughness testing in mode II—punch-through shear test. Int. J. Rock Mech. Miner. Sci. 41 (3).

Backers, T., Fardin, N., Dresen, G., Stephansson, O., 2003. Effect of loading rate on mode I fracture toughness, roughness and micromechanics of sandstone. Int. J. Rock Mech. Miner. Sci. 41 (3).

Backers, T., Dresen, G., Rybacki, E., Stephansson, O., 2004. New data on Mode II fracture toughness of rock from the punch-through shear test. In: SINOROCK 2004 Symposium, Paper 1A 01, Int. J. Rock Mech. Miner. Sci. 41(3).

Blandford, G.E., Ingraffea, A.R., Ligget, J.A., 1982. Two dimensional stress intensity factor computations using the boundary element method. Int. J. Numer. Methods Eng. 17, 387–404.

Bobet, A., 2001. A hybridized displacement discontinuity method for mixed mode I–II–III loading, Int. J. Rock Mech. Miner. Sci. 38, 1121–1134.

Broek, D., 1989. The Practical Use of Fracture Mechanics, fourth ed. Kluwer Academic Publishers, The Netherlands.

Carpinteri, A., Yang, G., 1997. Size effects in brittle specimen with microcrack interaction. Comput. Struct. 63, 429–437.

Cotterell, B., Rice, J.R., 1980. Slightly curved or kinked cracks. Int. J. Fract. Mech. 16, 155–169.

Crawford, A.M., Curran, J.H., 1982. Higher order functional variation displacement discontinuity elements. Int. J. Rock Mech. Miner. Sci. Geomech. Abstr. 19, 143–148.

Crouch, S.L., 1976. Solution of plane elasticity problems by the displacement discontinuity method. Int. J. Numer. Methods Eng. 10, 301–343.

Crouch, S.L., Starfield, A.M., 1983. Boundary Element Methods in Solid Mechanics. Allen and Unwin, London.

Erdogan, F., Sih, G.C., 1963. On the crack extension in plates under plane loading and transverse shear. J. Basic Eng. 85, 519–527.

Fowell, R.J., 1995. Suggested methods for determining mode I fracture toughness using Chevren notched Brazilian disc specimen. Int. J. Rock Mech. Miner. Sci. 32 (1), 57–64.

Guo, H., Aziz, N.I., Schmidt, R.A., 1990. Linear elastic crack tip modeling by displacement discontinuity method. Eng. Fract. Mech. 36, 933–943.

Guo, H., Aziz, N.I., Schmidt, R.A., 1992. Rock cutting study using linear elastic fracture mechanics. Eng. Fract. Mech. 41, 771–778.

Hwang, C.G., Ingraffea, A.R., 2004. Shape prediction and stability analysis of Mode-I planar cracks. Eng. Fract. Mech. 71, 1751–1777.

Huang, J., Wang, S., 1985. An experimental investigation concerning the comprehensive fracture toughness of some brittle rocks. Int. J. Rock Mech. Miner. Sci. Geomech. Abstr. 22, 99–104.

Ingraffea, A.R., 1981. Mixed-mode fracture initiation in Indiana Sandstone and Westerly Granite. In: Einstein, H.H. (Ed.), Rock Mechanics from Research to Application. Proceedings of the 22nd US Symposium in Rock Mechanics. MIT, Cambridge, MA, pp. 199–204.

Ingraffea, A.R., 1983. Numerical modeling of fracture propagation. In: Rossmanith, H.P. (Ed.), Rock Fracture Mechanics. Springer-Verlag, Wien, New York, pp. 151–208.

Ingraffea, A.R., 1987. Theory of crack initiation and propagation in rock. In: Atkinston, B.K. (Ed.), Fracture Mechanics of Rock, Geology Series. Academy Press, New York, pp. 71–110, pp. 151–208.

Ingraffea, A.R., Hueze, F.E., 1980. Finite element models for rock fracture mechanics. Int. J. Numer. Anal. Methods Geomech. 4, 25.

Ouchterlony, F., 1983. Analysis of cracks. In: Rossmanith, H.P. (Ed.), Rock Fracture Mechanics. Springer-Verlag, Wien, New York, pp. 31–67.

Ouchterlony, F., 1988. Suggested methods for determining the fracture toughness of rock, ISRM commission on testing methods. Int. J. Rock Mech. Miner. Sci. Geomech. Abstr. 25, 71–96.

Pang, H.L.J., 1995. Mixed mode fracture analysis and toughness of adhesive joints. Eng. Fract. Mech. 51, 575–583.
Rao, Q., Sun, Z., Stephansson, O., Li, C., Stillborg, B., 2003. Shear fracture (Mode II) of brittle rock. Int. J. Rock Mech. Miner. Sci. 40, 355–375.
Scavia, C., 1990. Fracture mechanics approach to stability analysis of crack slopes. Eng. Fract. Mech. 35, 889–910.
Scavia, C., 1992. A numerical technique for the analysis of cracks subjected to normal compressive stresses. Int. J. Numer. Methods Eng. 33, 929–942.
Scavia, C., 1995. A method for the study of crack propagation in rock structures. Geotechnics 45, 447–463.
Shen, B., Stephansson, O., 1994. Modification of the *G*-criterion for crack propagation subjected to compression. Eng. Fract. Mech. 47 (2), 177–189.
Shen, B., Stephansson, O., Rinne, M., Lee, H.-S., Jing, L., Roshoff, K., 2004. A fracture propagation code and its application to nuclear waste disposal. Int. J. Rock Mech. Miner. Sci. 41 (3), 448–453.
Shou, K.J., Crouch, S.L., 1995. A higher order displacement discontinuity method for analysis of crack problems. Int. J. Rock Mech. Miner. Sci. Geomech. Abstr. 32, 49–55.
Sih, G.C., 1973. Methods of analysis and solutions of crack ProblemsMech. Fract., vol. 1. Noordhoff International Publishing, Leyden.
Sneddon, I.N., 1951. Fourier Transforms. McGraw-Hill, New York.
Stephansson, O., 2002. Recent rock fracture mechanics developments. In: 1st Iranian Rock Mechanics Conference, pp. 675–698.
Stephansson, O., Backers, T., Dresen, G., Rybacki, E., 2001. Shear fracture mechanics of rocks and a new testing method for K_{IIC}. In: Sarkka P. & Eloranta P., (Eds.), Rocks Mechanics a Challenge for Society, Proceedings of the ISRM Regional Symposium, EUROCK 2001, Finland: EPSOO, pp. 163–168.
Sun, G.X., Whittaker, B.N., Sing, R.N., 1990. Use of Brazilian disc test for determination of the mixed Mode I–II Fracture toughness envelope of rock. In: International Conference on Mechanical of Jointed and Fractured Rocks, Vienna, Austria, pp. 18–20.
Swartz, S.E., Lu, L.W., Tang, L.D., Refai, T.M.E., 1988. Mode II fracture parameters estimates for concrete from beam specimens. Exp. Mech. 28, 46–53.
Tan, X.C., Kou, S.Q., Lindqvist, P.A., 1996. Simulation of rock fragmentation by indenters using DDM and fracture mechanics. In: Aubertin, M., Hassani, F., Mitri, H. (Eds.), Rock Mechanics, Tools and Techniques. Balkema, Roterdam.
Whittaker, B.N., Singh, R.N., Sun, G., 1992. Rock Fracture Mechanics, Principles, Design and Applications. Elsevier, The Netherlands.
Zipf, R.K., Bieniawski, Z.T., 1987. Development of the mixed mode testing system for geological materials. In: Shah, S.P., Swartz, S.E., (Eds.), SEM/RILEM International Conference on Fracture of Concrete and Rock, Houston, TX, pp. 338–352.